Photoionization from the $2p$ subshell of the laser-excited aligned Na^* $2p^63p$ $^2P_{3/2}$ state

D. Cubaynes,[1] S. Guilbaud,[1] F. J. Wuilleumier,[1] M. Meyer,[1] E. Heinecke,[2] K. Riek,[2] P. Zimmermann,[2] M. Yalçinkaya,[3] S. Fritzsche,[4,5] S. I. Strakhova,[6] and A. N. Grum-Grzhimailo[1,6]

[1]*LIXAM, Centre Universitaire Paris-Sud, Bâtiment 350, F-91405 Orsay Cedex, France*

[2]*Institut für Atomare Physik und Fachdidaktik, Technische Universität Berlin, Hardenbergstrasse 36, D-10623 Berlin, Germany*

[3]*Department of Physics, Science Faculty, Istanbul University, 34118 Vezneciler/Istanbul, Turkey*

[4]*GSI Helmholtzzentrum für Schwerionenforschung, D-64291 Darmstadt, Germany*

[5]*Department of Physical Sciences, University of Oulu, P.O. Box 3000, Fin-90014 Oulu, Finland*

[6]*Institute of Nuclear Physics, Moscow State University, Moscow 119991, Russia*

(Received 3 June 2009; published 14 August 2009)

High resolution angle-resolved photoelectron spectra from Na atoms laser excited and aligned in the Na^* $2p^63p$ $^2P_{3/2}$ state are investigated experimentally and theoretically in the region of the Na^+ $2p^53p$ manifold. A prominent influence of the alignment on the relative line intensities is observed. The measured linear alignment dichroism is in good agreement with the theoretical results obtained in the multiconfigurational Dirac-Fock approximation as well as in a generalized geometrical model, which is extended to the description of angular distributions of photoelectrons from polarized atoms.

DOI: 10.1103/PhysRevA.80.023410 PACS number(s): 32.80.Fb

I. INTRODUCTION

The combination of laser optical pumping with angle-resolved photoelectron spectroscopy in the xuv provides detailed insight into the dynamics of atomic photoionization from inner subshells [1]. Specific advantage can be taken from the possibility to change in a controlled way the electronic cloud of the atom before the ionization, i.e., to state prepare the atom by laser excitation. Photoionization of the $2p$ subshell from laser-excited Na^* $2p^63p$ states has been studied extensively and may be considered as a showcase for such type of investigations. The first measurements concentrated on the spectroscopy of the autoionizing states by methods of photoabsorption [2] and electron spectrometry from isotropic [3] and polarized [4,5] excited sodium atoms, while with increasing intensity of the synchrotron radiation (SR) sources photoelectron spectrometry was applied to the direct ionization [6–8] providing rich information on electron correlations and dynamics of the photoionization. Parallel to the experimental developments, the theoretical predictions for resonant and nonresonant photoionization in the crossed beams of an optical pumping laser and SR were worked out. In particular, first predictions for resonant photoionization were made [9], a theory of the photoelectron angular distributions was developed [10], and partial photoionization cross sections and asymmetry parameters in the photoelectron angular distributions were calculated in a many-body perturbation theory [11,12], multiconfiguration Hartree-Fock method [13], within a relaxed-orbital Hartree-Fock framework [14–18], and in an R-matrix approach [7].

Utilizing the high energy resolution of electron spectrometers and the high brightness of third generation SR sources allow nowadays to resolve the fine structure of the photoelectron lines and to study final-state-specific cross sections. Recently, high-resolution photoelectron spectra from laser-excited alkali-metal atoms in the $np^6(n+1)p$ $^2P_{1/2}$ and $^2P_{3/2}$ states were obtained experimentally and analyzed theoretically [8,19–22]. These studies were concentrating on the relative cross sections, while the influence of the alignment of the initial laser-excited $np^6(n+1)p$ $^2P_{3/2}$ states was minimized and/or neglected. In particular, the relative intensities of lines in the fine-structure-resolved $np^5(n+1)p$ photoelectron spectra in Na ($n=2$) and K ($n=3$) were explained by simple means within a generalized geometrical model [8,19]. From another side, photoionization of polarized atoms brings new information on the dynamics of the process, in some cases even up to the degree of "complete" photoionization experiment (for example [23–25]). The purpose of the present paper is to utilize the fact that the initial Na^* $2p^63p$ $^2P_{3/2}$ state is aligned, being excited by optical pumping with linearly polarized laser light, and to study experimentally and theoretically the dependence of the fine-structure resolved photoelectron spectrum on the direction of the alignment (i.e., the linear alignment dichroism) in order to obtain additional information on the photoionization dynamics. The influence of the polarization on the $2p$ photoionization of Na was already mentioned in [1] and a dependency of the intensity of the shakedown satellite lines from the direction of the alignment was observed in [26]. Here we concentrate on the diagram lines in the photoelectron spectrum and give a theoretical interpretation of the corresponding dependency. For the theoretical predictions, we apply first the conventional multiconfigurational Dirac-Fock (MCDF) model and, second, we extend the generalized geometrical model (GGM) to the description of the photoelectron angular distributions from polarized atoms.

The experimental details for measurements of the photoelectron spectra and of the linear alignment dichroism are given in Sec. II. Theoretical approaches are summarized in Sec. III, containing a description of the MCDF model and the GGM. The results and their analysis are presented in Sec. IV, followed by a summarizing conclusion. Atomic units are used throughout until otherwise indicated.

II. EXPERIMENT

The experiments were performed at beamline U125/2-SGM of the SR source BESSY II in Berlin (Germany). The

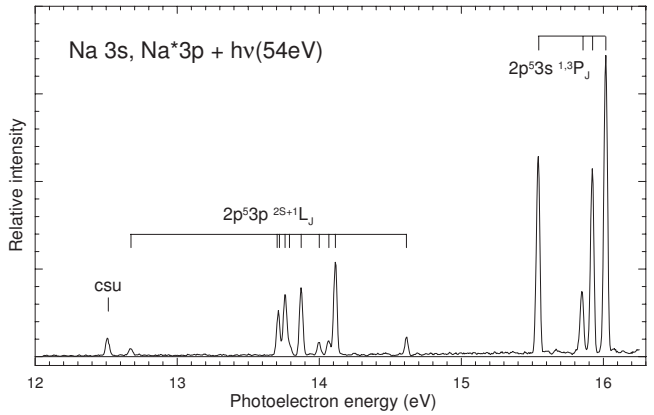

FIG. 1. Typical photoelectron spectrum recorded upon ionization at 54 eV photon energy in the $2p$ shell of sodium atoms in the $2p^63s$ ground state and in the $2p^63p$ laser-excited state. The line at 12.5 eV, labeled "csu," corresponds to the $^3S_1$ component of the $2p^53p$ conjugate shake-up satellite from the $2p$ ionization of the ground state.

counterpropagating laser and synchrotron radiation intersect a beam of sodium vapor, which is produced by a radiatively heated oven, in the source volume of a high-resolution electron energy analyzer (Scienta SES-2002) mounted at the magic angle (54°44′) with respect to the linear SR polarization vector. Electron spectra were recorded at different photon energies of 54 and 80 eV. The overall energy resolution of the spectra was measured at a photon energy of 54 eV to be about 27 meV, which comprises the resolution of about 20 meV for both the exciting synchrotron beam and the electron analyzer.

For the excitation of the sodium atoms, two continuous-wave single-mode ring dye lasers (Rhodamine 6G) were used to pump efficiently the Na $2p^63s\ ^2S_{1/2} \rightarrow \mathrm{Na}^*\ 2p^63p\ ^2P_{3/2}$ transition at $\lambda = 588.995$ nm. Both hyperfine components ($F=1$ and $F=2$) of the ground state were excited by tuning the wavelength of the lasers respectively to the $F=2 \rightarrow F'=3$ and the $F=1 \rightarrow F'=2$ transition, which are separated by 1.77 GHz. The laser beams were introduced in a quasicollinear way into the experimental chamber and focused by a convex lens of 60 cm focal length to a diameter of about 50 μm in the interaction region. In this way, using typical laser powers of 200 and 600 mW, about 40% of the atoms were pumped into the $\mathrm{Na}^*\ 2p^63p\ ^2P_{3/2}$ excited state.

A typical electron spectrum recorded with the SR at a photon energy of 54 eV and the laser wavelengths tuned to the $3s\ ^2S_{1/2} \rightarrow 3p\ ^2P_{3/2}$ transition is displayed in Fig. 1 for the kinetic energy region corresponding to the $2p$ ionization. The spectrum was taken for parallel linear polarization vectors of the lasers and SR. Photoionization of the ground state atoms gives rise to $\mathrm{Na}^+\ 2p^53s\ ^1P_1, {}^3P_{0,1,2}$ final ionic states in the kinetic energy region around 15.5–16.0 eV and to the $^3S_1$ component of the $\mathrm{Na}^+\ 2p^53p$ conjugate shake-up satellite at 12.5 eV. These lines were used to monitor the density of the Na vapor and the number of excited states, and to control the kinetic energy dependent transmission of the electron analyzer. The electron emission from the laser-excited atoms is clearly separated with respect to the kinetic energy, and the individual components of the final ionic states $2p^53p\ ^{1,3}(S,P,D)_{0,1,2,3}$ are well resolved.

Recording now spectra for different relative angles φ_a between the linear polarization vectors enables us to determine the so-called linear alignment dichroism (LAD). For the measurements, a rotatable Fresnel rhomb was installed in the optical path allowing to control the relative orientation of the laser polarization with respect to that of the SR, in particular to set it to the values 0°, 90°, −45°, and +45°, where $\varphi_a = 0°$ corresponds to parallel polarization vectors of laser and SR. The precision of adjusting the laser polarization at a specific angle was estimated to be better than ±2°. The LAD is then defined as the difference between two spectra recorded for two different angles φ_a

$$\mathrm{LAD}(\varphi_{a,1}|\varphi_{a,2}) = I(\varphi_{a,1}) - I(\varphi_{a,2}), \tag{1}$$

where I stands for the intensity of the photoelectron flux at the fixed detector position.

The main difficulty of the measurements is given by the need for a long-term stability of several parameters, in particular of the number of the excited atoms which critically depends on the wavelength stability of the laser and the spatial stability of the overlap between the laser and SR beams.

III. THEORY

A. General considerations

We consider atomic photoionization described by

$$\gamma + A(\alpha_i J_i) \rightarrow [A^+(\alpha_f J_f) + e^-_{\mathrm{ph}}(\ell j)]J, \tag{2}$$

where J_i (J_f) is the total angular momentum of the initial atomic (final ionic) state, the sets of quantum numbers α_i (α_f) are introduced to completely characterize these states, ℓ and j are the orbital and the total angular momenta of the photoelectron, respectively, and J is the total angular momentum of the channel ($\boldsymbol{J}=\boldsymbol{J}_f+\boldsymbol{j}$). Using the results of [10] for the geometry of the present experiment, the differential photoionization cross section can be cast into the form (for $J_i < 2$),

$$\left(\frac{d\sigma}{d\Omega}\right)_{if} = \frac{\sigma_{if}}{4\pi}[1 + \mathcal{A}_{20}(B + B_c \cos 2\varphi_a + B_s \sin 2\varphi_a)], \tag{3}$$

where σ_{if} is the angle-integrated photoionization cross section for the $\alpha_i J_i \rightarrow \alpha_f J_f$ transition from randomly oriented atoms, $\mathcal{A}_{20}$ is the alignment parameter of the angular momentum J_i of the initial atomic state, and the parameters B, B_s, and B_c are defined by

$$B = -\frac{\sqrt{10}}{4\sqrt{3}}\beta_{202} + \frac{\sqrt{5}}{4\sqrt{3}}\beta_{220} - \frac{5\sqrt{7}}{14\sqrt{3}}\beta_{222} - \frac{\sqrt{35}}{28\sqrt{3}}\beta_{242}, \tag{4}$$

$$B_s = \frac{\sqrt{10}}{2\sqrt{3}}\beta_{220} + \frac{5\sqrt{14}}{14\sqrt{3}}\beta_{222} + \frac{5\sqrt{70}}{42\sqrt{3}}\beta_{242}, \tag{5}$$

$$B_c = -\frac{3\sqrt{10}}{4\sqrt{3}}\beta_{202} - \frac{\sqrt{5}}{4\sqrt{3}}\beta_{220} + \frac{5\sqrt{7}}{14\sqrt{3}}\beta_{222} + \frac{31\sqrt{35}}{84\sqrt{3}}\beta_{242}. \tag{6}$$

All information about the dynamics of the photoionization process and about the atomic structure is contained in the anisotropy parameters $\beta_{k_0kk_\gamma}$, which are given in terms of the reduced dipole photoionization amplitudes $D_{\alpha_f J_f,\ell j:J} \equiv \langle \alpha_f J_f, \ell j:J||D||\alpha_i J_i\rangle$ by

$$\beta_{k_0kk_\gamma} = 3\hat{J}_i N^{-1} \sum_{\substack{JJ'\\ \ell\ell' jj'}} (-1)^{J+J_f+k_\gamma-1/2}\hat{J}\hat{J}'\hat{j}\hat{j}'\hat{\ell}\hat{\ell}'(\ell 0,\ell' 0|k0) \times \begin{Bmatrix} j & \ell & \frac{1}{2} \\ \ell' & j' & k \end{Bmatrix} \begin{Bmatrix} j & J & J_f \\ J' & j' & k \end{Bmatrix} \times \begin{Bmatrix} J_i & 1 & J \\ J_i & 1 & J' \\ k_0 & k_\gamma & k \end{Bmatrix} D_{\alpha_f J_f,\ell j:J} D^*_{\alpha_f J_f,\ell' j':J'}, \tag{7}$$

where $N=\Sigma_{\ell jJ}|D_{\alpha_f J_f,\ell j:J}|^2$, $\hat{a} \equiv \sqrt{2a+1}$ and standard notations are used for the Clebsch-Gordan coefficients, 6-j, and 9-j Wigner coefficients.

The LAD(0|90) and LAD(45|−45) [see Eq. (1)] are proportional to the corresponding differences of the cross sections [Eq. (3)] and are distinguished owing to their relative simplicity, which is the result of cancellation of several terms in comparison to Eq. (3). Namely, one obtains

$$\text{LAD}(0|90) = \frac{\sigma_{if}}{4\pi} 2\mathcal{A}_{20} B_c,$$

$$\text{LAD}(45|-45) = \frac{\sigma_{if}}{4\pi} 2\mathcal{A}_{20} B_s, \tag{8}$$

assuming that the observed spectra are normalized to the differential photoionization cross section [Eq. (3)].

B. Multiconfigurational Dirac-Fock approximation

The MCDF method has been outlined in detail in the literature (for example, [27]) and does not need a detailed discussion here, except particular points related to the present calculations. Computations are based on the RATIP code [28,29]. The initial atomic state, Na^* $2p^6 3p\ ^2P_{3/2}$, and the final ionic states, Na^+ $2p^5 3p$, were described by the configuration mixtures $2p^6 3p + 2p^6 4p + 2s2p^6 3s3p + 2p^5 3p^2$ and $2p^5 3p + 2p^5 4p + 2p^6 + 2s2p^6 3s$, respectively. The electron orbitals were optimized independently for the atomic and ionic states. It is known that strong relaxation effects occur in sodium due to the nonorthogonality of the atomic and ionic orbitals with the same symmetry, giving rise to strong satellite lines in the photoelectron spectra [6,15]. Therefore, in the photoionization amplitudes $D_{\alpha_f J_f,\ell j:J}$, the nonorthogonality was taken into account between the atomic and ionic orbitals of the same symmetry. The electron wave functions (spinors) for the discrete spectrum were computed using the GRASP92 code [30], while the continuum spinors and their coupling to the bound-state electrons are generated "on fly" in course of the computation by means of the RATIP procedures (see [31,32]). The frozen core approximation with accounting for the electron exchange was used for the continuum. Calculations without taking into account the nonorthogonality of atomic and ionic orbitals and in the single configuration approximation were performed for comparison. Although the absolute values of the photoionization cross sections are sensitive to relaxation effects and configuration mixing, the ratios of the partial photoionization amplitudes change only slightly. An exception is the upper state of the Na^+ $2p^5 3p$ configuration with $J_f=0$, where the admixture of configurations noticeably influences the photoionization cross section relative to those for other ionic final states. Additional accounting for the relaxation partly compensates the above effect of the configuration mixing for this state.

In the MCDF approximation, the continuum electron function is specific for each channel, which is described by the set of quantum numbers $\{\alpha_f, J_f, \ell, j, J\}$ and the photoelectron energy E, giving in total 64 generally independent complex amplitudes for photoionization into states of the Na^+ $2p^5 3p$ manifold. The MCDF calculations of the cross sections and the LAD proceed using the explicit formulas (3)–(8). But due to the large number of channels, essential physics can be hidden behind these cumbersome expressions. For an easier understanding of the results, it is therefore instructive to develop a simpler model, which keeps general trends of the more accurate approach. Such a model is given by the GGM [8,19], which has been used successfully in the description of the relative intensities of lines in the fine-structure resolved photoelectron spectra from isotropic atoms. For the description of the LAD, we shall extend the GGM to the case of polarized atoms in the next section.

C. Generalized geometrical model

The GGM is based on a standard treatment of photoionization from many-electron atoms (for example [33]); it accounts for the intermediate coupling in the final ionic and initial atomic states, but neglects mixing of configurations and the dependence of electron wave functions on the global quantum numbers. When the relativistic splitting of the $E\ell j$ continuum wave functions is also neglected, the dynamics of the photoionization is fully determined by two single-particle complex amplitudes

$$D_\ell \equiv \langle E\ell||d||n_i\ell_i\rangle = i^{-\ell}e^{i\sigma_\ell}(\sqrt{\ell}\,\delta_{\ell,\ell_i+1} - \sqrt{\ell+1}\,\delta_{\ell,\ell_i-1}) \int_0^\infty dr P_{E\ell}(r) r P_{n_i\ell_i}(r), \tag{9}$$

similar to the three-parameter (Cooper-Zare) model [34]. Here σ_ℓ is the scattering phase, $P_{n_i\ell_i}(r)$ and $P_{E\ell}(r)$ are radial functions of the electron in the initial state $n_i\ell_i$ (in our case $n_i\ell_i=2p$) and in the continuum state $E\ell$, respectively. The GGM implies that the amplitudes D_ℓ do not change within the spectral range of the multiplet splitting of the final ionic configuration. With these approximations one obtains for $\beta_{k_0kk_\gamma}$ [Eq. (7)] after standard algebra [35,36]

$$\beta_{k_0 k k_\gamma} = \sqrt{3}\frac{C_{k_0}(\alpha_f J_f)}{C_0(\alpha_f J_f)}\frac{b_{k_0 k k_\gamma}}{b_{000}}, \tag{10}$$

where the one-electron parameters $b_{k_0 k k_\gamma}$ are expressed in terms of the amplitudes [Eq. (9)] by Eq. (20) of [37]. The constants $C_{k_0}(\alpha_f J_f)$ depend only on the quantum numbers of the initial atomic and final ionic states and the mixing coefficients,

$$C_{k_0}(\alpha_f J_f) = \frac{3\hat{J}_i^3 \hat{J}_f^2}{\hat{S}_i^2}\sum_x (-1)^{J_i+x+\ell_i}\hat{x}^2 \begin{Bmatrix} J_i & J_i & k_0 \\ \ell_i & \ell_i & x \end{Bmatrix} \times \left(\sum_{L_f S_f} \gamma_{L_f S_f}^{\alpha_f J_f}(-1)^{J_f+L_f+S_f}\hat{L}_f\hat{S}_f \begin{Bmatrix} J_f & L_f & S_f \\ S_i & \frac{1}{2} & x \end{Bmatrix} \times \begin{Bmatrix} J_i & S_i & L_i \\ L_f & \ell_i & x \end{Bmatrix} \right)^2. \tag{11}$$

We have assumed that the initial atomic state is described in the pure *LSJ*-coupling scheme, while the ionic states are described by the intermediate coupling wave functions, i.e., a superposition of the *LSJ*-coupled wave functions through $|\alpha_f J_f\rangle = \Sigma_{L_f S_f} \gamma_{L_f S_f}^{\alpha_f J_f} |\alpha_f L_f S_f J_f\rangle$, where $\gamma_{L_f S_f}^{\alpha_f J_f}$ are the mixing coefficients. Equation (11) is written for ionization from the closed $n_i \ell_i$ subshell with a single "spectator" electron on an unoccupied subshell. An expression for the coefficients $C_{k_0}(\alpha_f J_f)$ in the case of intermediate coupling in both initial atomic and final ionic states is presented in [38].

An earlier study [37] represents a particular case of the present results for the pure *LSJ*-coupling scheme. For example, the product form (10) generalizes Eq. (21) of [37] to the case of intermediate coupling and Eq. (26) of [37] is a limiting case of Eq. (11) for pure *LSJ*-coupling. Finally, for $k_0=0$, Eq. (11) turns, for alkali-metal atoms, into Eq. (1) of [8] for the integral cross section (where the equivalent result is written in terms of 9-*j* symbols). Thus, Eqs. (10) and (11) extend the GGM for the cross sections to the angular distribution of photoelectrons from polarized atoms.

A compact expression can be obtained for the differential cross section [Eq. (3)] for arbitrary final ionic states of the Na^+ $2p^5 3p$ manifold when taking Eq. (10) into account,

$$\left(\frac{d\sigma}{d\Omega}\right)_{if} = \frac{\sigma_{if}}{4\pi}\left[1 - \frac{T_f}{2}\left(1 + 3\frac{1-z^2}{1+z^2}\cos 2\varphi_a - 6\frac{z\cos\Delta}{1+z^2}\sin 2\varphi_a\right)\right], \tag{12}$$

which contains two real dimensionless photoionization parameters, the absolute amplitude ratio $z=|D_d|/|D_s|$, and the phase difference $\Delta=\sigma_d-\sigma_s$. The final-state-specific integral cross sections and the constants in Eq. (12) are given, respectively, by

$$\sigma_{if} = \tfrac{1}{2} C_0(\alpha_f J_f)\sigma_{2p} \tag{13}$$

and

$$T_f = \frac{1}{\sqrt{2}}\frac{C_2(\alpha_f J_f)}{C_0(\alpha_f J_f)}\mathcal{A}_{20}, \tag{14}$$

where

$$\sigma_{2p} = \frac{4\pi^2\alpha\omega}{3}\frac{1}{3\sqrt{3}}(|D_s|^2 + |D_d|^2) \tag{15}$$

is the single-electron 2p-photoionization cross section, α is the fine-structure constant, and ω is the photon energy. Furthermore, as follows from Eq. (12), the LAD for any photoelectron line in the manifold is expressed by the relations

$$\mathrm{LAD}(0|90) = \frac{\sigma_{2p}}{4\pi}C_2(\alpha_f J_f)\mathcal{A}_{20}\frac{3}{\sqrt{2}}\frac{1}{2}\frac{z^2-1}{z^2+1}, \tag{16}$$

$$\mathrm{LAD}(45|-45) = \frac{\sigma_{2p}}{4\pi}C_2(\alpha_f J_f)\mathcal{A}_{20}\frac{3}{\sqrt{2}}\frac{z\cos\Delta}{z^2+1}, \tag{17}$$

which can be analyzed easily. Noteworthy, the LAD$(0|90)$ depends, within the GGM, only on the absolute ratio of the two amplitudes, while the LAD$(45|-45)$ includes the relative phase of the amplitudes. For numerical calculations in the GGM, the same Hartree-Fock values of mixing coefficients $\gamma_{L_f S_f}^{\alpha_f J_f}$ were used as in [8,19], which provided a good description of the photoelectron spectrum in the region of the Na^+ $2p^5 3p$ manifold. Particular values of the parameters z and Δ will be discussed in Sec. IV B. In both models, the MCDF and the GGM, we used experimental binding energies to display the LAD on an energy axis.

IV. RESULTS AND DISCUSSION

A. Alignment of the laser-excited state

For the quantitative analysis of the photoionization process, the value of the alignment, $\mathcal{A}_{20}$, of the initial Na^* $2p^6 3p\ ^2P_{3/2}$ state has to be known. Note that some "effective" alignment of the target atom is implied, which depends on the geometry of the reaction volume and can be sensitive to minor changes in the experimental conditions, such as fluctuations of the target density and laser power, or Doppler broadening of the hyperfine levels. The alignment of the excited state can be monitored by the observation of the fluorescence polarization [39], or, as it is done in the present study, by measuring for resonant photoionization the modulation of the photoelectron intensity when rotating the linear polarization of the exciting laser light [4].

For the case of the Na^{**} $[2p^5(^2P)3s3p(^3P)]^2S_{1/2}$ resonance at $h\nu(\mathrm{SR})=31.78$ eV, the only open electronic decay channel is autoionization into the Na^+ $2p^6\ ^1S_0$ final ionic state. The intensity of the photoelectrons, which are produced after photoexcitation by linearly polarized SR to the autoionizing state with angular momentum $J_r=\frac{1}{2}$ and which are observed under the magic angle between the directions of the electron emission and the SR polarization, can be described [4,10] up to an irrelevant constant c in the form

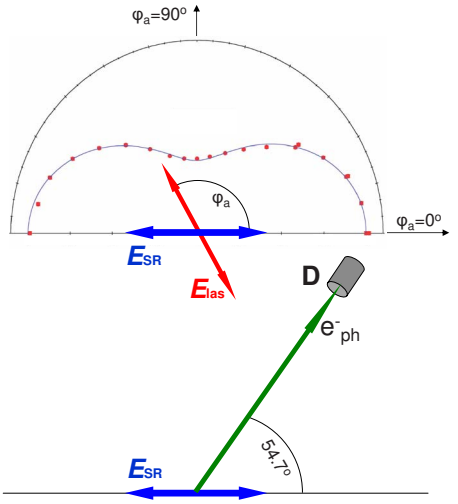

FIG. 2. (Color online) (Bottom) Geometry of the experimental setup. (Top) φ_a scan of the photoelectron flux at the fixed position of the electron detector D for the photon energy of 31.78 eV corresponding to the photoexcitation of the Na** $2p^5 3s3p\ ^2S_{1/2}$ autoionizing state. The best fit according to Eq. (18) is shown providing the alignment of $\mathcal{A}_{20}=-0.64\pm0.01$.

$$I(\varphi_a) = c\left[\left(1-\frac{1}{4}\mathcal{A}_{20}\right) - \frac{3}{4}\mathcal{A}_{20}\cos 2\varphi_a\right]. \qquad (18)$$

Figure 2 shows the modulation of the photoelectron intensity upon excitation and decay of the Na** $2p^5 3s3p\ ^2S_{1/2}$ autoionizing state together with the geometry of our measurements, which were performed in the plane perpendicular to the photon beams. The best fit of the experimental data points by Eq. (18) results in $\mathcal{A}_{20}=-0.64\pm0.01$, which is very close to the stationary limit of $\mathcal{A}_{20}=-\frac{2}{3}$ for laser pumping by linearly polarized light to the final $3p\ ^2P_{3/2}$, $F=3$ hyperfine level. We note that the fitting procedure provides also a determination of the angle between the polarization vectors of laser and SR, which in the present experiment could be adjusted with a precision of $0.3\pm0.1°$.

B. Linear alignment dichroism

Typical electron spectra recorded for $\varphi_a=0°$ and $\varphi_a=90°$ are displayed in Fig. 3. Only the kinetic energy region corresponding to the 2p photoionization of excited Na atoms into the Na$^+$ $2p^5 3p\ ^{1,3}L_J$ final states is shown. The individual multiplet lines are well resolved with the exception of the $^3P_0$ and $^3P_1$ components, which are separated by only 1.5 meV, and appear as one line. The $^1P_1$ is seen as a shoulder to the $^3P_2$ and can easily be separated by a fitting procedure. Almost all lines show a pronounced intensity change with respect to the relative orientation of the linear polarization vectors, indicating thereby the influence of the alignment of the laser-excited Na* $2p^6 3p\ ^2P_{3/2}$ state on the photoionization from the $2p^6$ shell.

In order to visualize more clearly the effect for the individual lines, the LAD(0|90), Eq. (1), is shown in Fig. 4, where it is compared to the theoretical results obtained within the MCDF model and the GGM. On top of the figure,

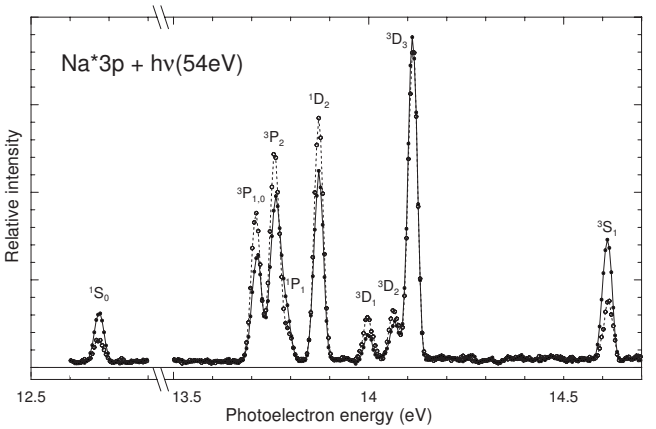

FIG. 3. Two photoelectron spectra of sodium atoms laser excited to the Na* $2p^6 3p\ ^2P_{3/2}$ state recorded at a photon energy of $h\nu=54$ eV for parallel, i.e., $\varphi_a=0°$ (open circles and dashed line) and perpendicular, i.e., $\varphi_a=90°$ (filled circles and solid line) orientation of the linear polarization vectors of laser and SR.

the difference of the two experimental spectra of Fig. 3 is presented. In comparison to the photoelectron spectrum, where eight peaks are observed in the energy region of the Na$^+$ $2p^5 3p$ manifold (cf. Fig. 3), nine features can be distinguished in the LAD(0|90). The overlapping lines $^3P_2$ and $^1P_1$ are clearly resolved in the dichroism patterns, since their dichroism is of opposite sign. This demonstrates the high

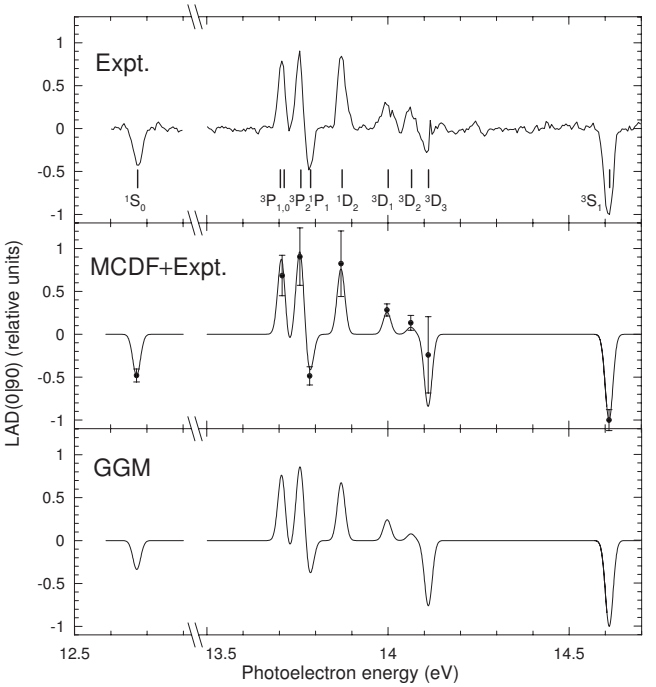

FIG. 4. LAD(0|90) at $h\nu=54$ eV for photoemission under the magic angle of 54.7° with respect to the SR electric field vector. Upper panel: experimental spectrum of the dichroism; middle panel: MCDF together with the experimental data for photoelectron lines; lower panel: GGM. Theoretical bar spectra of the LAD were convoluted by a Gaussian function with FWHM of 25 meV. Experiment and theory are normalized to −1 for the isolated $^3S_1$ line at 14.61 eV.

TABLE I. Factors $C_2(\alpha_f J_f)$ for the Na^+ $2p^5 3p$ states. Values of $C_2(L_f,S_f,J_f)$ for the pure *LSJ*-coupled states are given for comparison.

	$^1S_0$	$^3S_1$	$^1P_1$	$^3P_0$	$^3P_1$	$^3P_2$	$^1D_2$	$^3D_1$	$^3D_2$	$^3D_3$
$C_2(\alpha_f J_f)$	0.380	1.127	0.454	0.232	−0.940	−0.987	−0.762	−0.273	−0.089	0.857
$C_2(L_f,S_f,J_f)$	0.408	1.225	−0.612	0.204	0	−2.041	0.204	−0.245	0	0.857

sensitivity of dichroism measurements, showing that in our case the LAD reveal more details about the photoionization process from laser-excited atoms than the photoelectron spectrum.

In the middle panel of Fig. 4, the experiment is compared to the result of the MCDF calculations. The experimental values are presented here as solid circles indicating the differences in the integrated intensity under each line in the photoelectron spectrum. The unresolved $^3P_0$ and $^3P_1$ final states are shown as one data point. This type of presentation provides also information about the experimental accuracy, which is important in the comparison with theory. For the theoretical curves, the results were convoluted with Gaussian profiles of full width at half maximum of 25 meV taking into account the experimental broadening. The general structure of the experimental (top panel) and theoretical (middle and bottom panels) curves are in very good agreement. The sign and magnitude of the dichroism for each individual state are well described by both theoretical approaches. The main differences between experiment and theory are found for the $^3D_3$ line, which shows a less pronounced LAD(0|90) in the experiment than in theory.

When the two theoretical models are compared with each other, we note that the application of the GGM to the description of the LAD is quite successful: the GGM for the relative LAD(0|90) gives results almost identical to the MCDF, except for the line $^1S_0$. For this line, the LAD(0|90) in the GGM is ~30% less than in the MCDF due to strong configuration mixing, which is neglected in the GGM. Similar to the cases of pure coupling schemes [37,40], relative values and signs of the LAD of the photoelectron lines are completely governed by the $C_2(\alpha_f J_f)$ factors [see Eqs. (16) and (17)]. The $C_2(\alpha_f J_f)$ factors, calculated according to Eq. (11), are given in Table I together with the *LSJ*-coupled factors $C_2(L_f,S_f,J_f)$ from Eq. (26) of [37]. The values of $C_2(\alpha_f J_f)$ in the GGM differ drastically from $C_2(L_f,S_f,J_f)$ for the $^{1,3}P_1$, $^3P_2$, $^1D_2$ states, sometimes even changing the sign. The fact that they provide correct LAD(0|90) spectral pattern at the corresponding photoelectron energies of 13.6–13.9 eV (Fig. 4) is consistent with the statement that the intermediate coupling scheme is more adequate than *LSJ*-coupling scheme (cf. [8]). In particular, the given $C_2(\alpha_f J_f)$ show directly the observed difference in sign of the LAD(0|90) for the $^1S_0$, $^1P_1$, $^3D_3$, and $^3S_1$ states with respect to the other lines. The dichroism pattern in Fig. 4 differs significantly from regular LAD patterns for initial atomic states with *S* symmetry, which show three lobes of alternating sign and two nodes [37]. These regular patterns were based on certain properties of the 6-*j* symbols combined with the Landé interval rule; both these issues are not relevant to the present study, where the ionization from a state of *P* symmetry is treated in intermediate coupling. Furthermore, the LAD summed up separately for singlet and triplet Na^+ $2p^5 3p$ states does not vanish and therefore the "sum rule 2," formulated in [37] for the pure coupling scheme and states with symmetries other than the *S* symmetry, is violated.

The second experimental data set concerns the photoelectron spectra recorded at $\varphi_a = +45°$ and $\varphi_a = -45°$. The LAD(45|−45) is much less pronounced then the LAD(0|90) leading to rather large error bars for the experimental results (Fig. 5). Therefore only the differences in the integrated experimental line intensities are given. In general, the tendencies are again well reproduced by the theoretical models, although due to the small differences in the electron spectra, the quality of the experimental results is not good enough to give a clear guidance for theory.

The observed reduced sensitivity for the LAD(45|−45) is well predicted by theory. Indeed, within the GGM, the LAD(0|90) and LAD(45|−45) [Eqs. (16) and (17)] differ by the same factor

$$\xi = \frac{\mathrm{LAD}(0|90)}{\mathrm{LAD}(45|-45)} = \frac{z^2-1}{2z\cos\Delta} \tag{19}$$

for all photoelectron lines of the Na^+ $2p^5 3p$ configuration. In the single configuration frozen core Hartree-Fock calculations by the MCHF code [41], we obtain a value of $z \simeq 3.4$ for the ratio of the *d* and *s* channel amplitudes. This value is almost independent on the global quantum numbers of the ionization channel and on the energy of the photoelectron within the Na^+ $2p^5 3p$ configuration. This value of *z* is in accordance with earlier results of Chang [11] and Kupliauskiene [15], as follows from their curves for the partial photoionization cross sections. The phase difference Δ, as

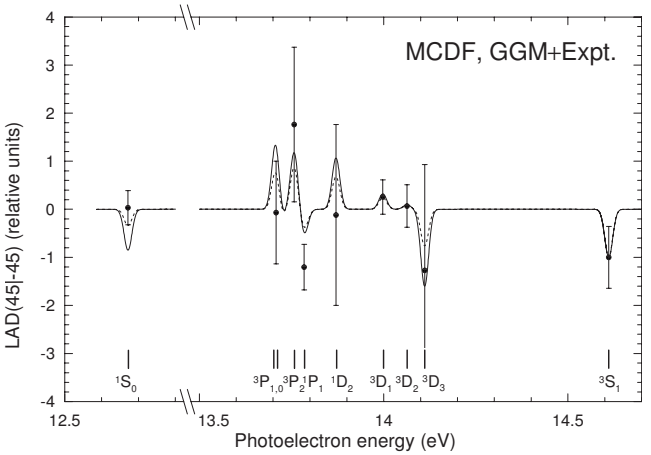

FIG. 5. Same as Fig. 4, but for LAD(45|−45). MCDF, solid; GGM, dashed.

obtained by the MCDF method, varies in the interval $1.2 \lesssim \Delta \lesssim 1.4$ from channel to channel and as function of the photoelectron energy, indicating a potential breakdown of the GGM for quantities depending on the relative phases of the photoionization amplitudes. With these values for z and Δ, the factor (19) takes the value of $\xi \simeq +5.8$. This large number explains why the LAD(45|−45) is much less pronounced than the LAD(0|90), while its positive sign explains why signs of the LAD(0|90) and LAD(45|−45) are the same.

Deviations between GGM and MCDF are larger for the LAD(45|−45) than for LAD(0|90), which is not unexpected due to the above discussion on the sensitivity of the former quantity to the relative phase Δ.

Generally, according to Eq. (17), the LAD(45|−45) vanishes when either one of the channels is dominating ($|z| \gg 1$ or $|z| \approx 0$) or the s and d channel amplitudes are orthogonal ($\Delta \approx \pm \frac{\pi}{2}$). Therefore, it would be interesting to study for example the $3p$ ionization of K atoms laser-aligned in the K^* $3p^6 4p\ ^2P_{3/2}$ state. The Cooper minimum in the d amplitude should lead to drastic effects in the LAD(0|90) to LAD(45|−45) ratio, Eq. (19), with changing the photon energy in the interval 40–65 eV.

Finally, a note on the complete experiment for photoionization from the $2p$ subshell of Na^* $2p^6 3p$ is appropriate in the context of the present data. It is instructive to discuss the complete experiment only within the GGM, i.e., with the set of the dynamical parameters z and Δ and implying that the values of the appropriate factors, Eq. (11), are determined beforehand, e.g., by independent calculations. A single measured LAD, Eq. (1), is not enough to extract the dynamical parameters, z and Δ, since the energy pattern of the LAD, i.e., the relative strength of the lines, does not depend on the photoionization amplitudes, as clearly emphasized already in [38]. In order to obtain the experimental information about the parameter z from the present data, one can normalize the measured LAD(0|90), Eq. (16), to the sum $I(0)+I(90)$, which depends on the state-specific constant T_f, Eq. (14), but is independent of z and Δ [42],

$$\frac{I(0)-I(90)}{I(0)+I(90)} = \frac{3T_f}{2-T_f}\frac{1-z^2}{1+z^2}. \tag{20}$$

If the constants T_f (and therefore the alignment $\mathcal{A}_{20}$) are known, in principle the value of z^2 can be extracted from the ratio (20) for any line of the multiplet. In practice, however, such an extraction procedure gives large uncertainties due to a denominator close to zero in the corresponding expression for z^2. For example, when applying Eq. (20) to the $^3S_1$ line, which shows a strong dichroic effect and is well separated from all other lines (cf. Fig. 4), a value of $z=3.2\pm2.6$ was determined. Also, only the positive sign of cos Δ, but not its absolute value could be deduced from the experimental LAD(45|−45) curve (cf. Fig. 5).

V. CONCLUSION

We performed high-resolution electron spectroscopic measurements for photoionization of laser excited and aligned sodium atoms in the $2p^6 3p\ ^2P_{3/2}$ state at the photon energy of 54 eV from the $2p$ subshell. Effects of the initial alignment on the photoelectron fine-structure spectra were observed and analyzed in direct photoionization from the inner shell. The calculations in the multiconfigurational Dirac-Fock approximation are in good agreement with the spectra, measured at different angles between the polarization vectors of the laser and synchrotron radiation beams. A generalized geometrical model is extended for treating angular distributions of photoelectrons from polarized atoms and successfully applied to explain general trends in the observed spectra and linear alignment dichroism. Spectral patterns of the linear alignment dichroism are well reproduced in our case without knowing the photoionization amplitudes explicitly: all what is needed are the intermediate coupling mixing coefficients and energies of the final ionic states.

ACKNOWLEDGMENTS

The project was funded by the European Community through the Research Infrastructure Action under the FP6 Structuring European Research Area Programme (Contract No. R II 3-CT-2004-506008). M.Y. acknowledges support by the DAAD. A.N.G gratefully acknowledges the hospitality of LIXAM Laboratory and of the Université Paris-Sud. S.F. acknowledges the support by the DFG under the project No. FR 1251/13.

[1] F. J. Wuilleumier and M. Meyer, J. Phys. B **39**, R425 (2006).
[2] J. Sugar, T. B. Lucatorto, T. J. McIlrath, and A. W. Weiss, Opt. Lett. **4**, 109 (1979).
[3] J. M. Bizau, F. Wuilleumier, D. L. Ederer, J. C. Keller, J. L. LeGouët, J. L. Picqué, B. Carré, and P. M. Koch, Phys. Rev. Lett. **55**, 1281 (1985).
[4] S. Baier, M. Schulze, H. Staiger, P. Zimmermann, C. Lorenz, M. Pahler, J. Rüder, B. Sonntag, J. T. Costello, and L. Kiernan, J. Phys. B **27**, 1341 (1994).
[5] S. Baier, M. Schulze, H. Staiger, M. Wedowski, P. Zimmerman, C. Lorenz, J. Rüder, M. Pahler, and B. Sonntag, J. Phys. B **28**, L81 (1995).
[6] D. Cubaynes, J. M. Bizau, F. J. Wuilleumier, B. Carré, and F. Gounand, Phys. Rev. Lett. **63**, 2460 (1989).
[7] B. Rouvellou, J.-M. Bizau, D. Cubaynes, J. Novak, M. Pahler, L. Journel, F. J. Wuilleumier, L. VoKy, P. Faucher, A. Hibbert, and N. Berrah, Phys. Rev. Lett. **75**, 33 (1995).
[8] D. Cubaynes, M. Meyer, A. N. Grum-Grzhimailo, J.-M. Bizau, E. T. Kennedy, J. Bozek, M. Martins, S. Canton, B. Rude, N. Berrah, and F. J. Wuilleumier, Phys. Rev. Lett. **92**, 233002 (2004).
[9] V. V. Balashov, A. N. Grum-Grzhimailo, and B. Zadamba, Opt. Spectrosc. **65**, 315 (1988).
[10] S. Baier, A. N. Grum-Grzhimailo, and N. M. Kabachnik, J.

Phys. B **27**, 3363 (1994).
[11] T. N. Chang and Y. S. Kim, J. Phys. B **15**, L835 (1982).
[12] T. N. Chang and Y. S. Kim, *Proceedings of the International Conference on X-Ray and Atomic Inner Shell Physics*, AIP Conf. Proc. No. 94, edited by B. Crasemann (AIP, New York, 1982), p. 633.
[13] H. P. Saha, Phys. Rev. A **50**, 3157 (1994).
[14] A. V. Kupliauskien, J. Phys. B **27**, 5647 (1994).
[15] A. Kupliauskiene, Phys. Scr. **53**, 149 (1996).
[16] A. Kupliauskiene, J. Phys. B **34**, 345 (2001).
[17] N. Rakštikas and A. Kupliauskiene, Phys. Scr. **58**, 587 (1998).
[18] A. Kupliauskiene and K. Glemza, J. Phys. B **35**, 4637 (2002).
[19] M. Meyer, D. Cubaynes, F. J. Wuilleumier, E. Heinecke, T. Richter, P. Zimmermann, S. I. Strakhova, and A. N. Grum-Grzhimailo, J. Phys. B **39**, L153 (2006).
[20] J. Schulz, M. Tchaplyguine, T. Rander, H. Bergersen, A. Lindblad, G. Öhrwall, S. Svensson, S. Heinäsmäki, R. Sankari, S. Osmekhin, S. Aksela, and H. Aksela, Phys. Rev. A **72**, 032718 (2005).
[21] J. Schulz, M. Määttä, S. Heinäsmäki, M. Huttula, R. Sankari, E. Kukk, T. Rander, S. Svensson, S. Aksela, and H. Aksela, Phys. Rev. A **73**, 062721 (2006).
[22] K. Jänkälä, J. Schulz, M. Huttula, A. Calò, S. Urpelainen, S. Heinäsmäki, S. Fritzsche, S. Svensson, S. Aksela, and H. Aksela, Phys. Rev. A **74**, 062704 (2006).
[23] H. Klar and H. Kleinpoppen, J. Phys. B **15**, 933 (1982).
[24] K. Godehusen, P. Zimmermann, A. Verweyen, A. von dem Borne, Ph. Wernet, and B. Sonntag, Phys. Rev. A **58**, R3371 (1998).
[25] G. Prümper, B. Zimmermann, B. Langer, J. Viefhaus, R. Hentges, N. A. Cherepkov, B. Schmidtke, M. Drescher, U. Heinzmann, U. Becker, and H. Kleinpoppen, Phys. Rev. Lett. **85**, 5074 (2000).
[26] J. Schulz, M. Tchaplyguine, T. Rander, O. Björneholm, S. Svensson, R. Sankari, S. Heinäsmäki, H. Aksela, S. Aksela, and E. Kukk, Phys. Rev. A **72**, 010702(R) (2005).
[27] I. P. Grant, in *Methods in Computational Chemistry*, edited by S. Wilson (Plenum Press, New York, 1988), Vol. 2, p. 1.
[28] S. Fritzsche, J. Electron Spectrosc. Relat. Phenom. **114-116**, 1155 (2001).
[29] S. Fritzsche, H. Aksela, C. Z. Dong, S. Heinäsmäki, and J. E. Sienkiewicz, Nucl. Instrum. Methods Phys. Res. B **205**, 93 (2003).
[30] F. A. Parpia, C. Froese Fischer, and I. P. Grant, Comput. Phys. Commun. **94**, 249 (1996).
[31] S. Fritzsche, A. Surzhykov, and T. Stöhlker, Phys. Rev. A **72**, 012704 (2005).
[32] S. Fritzsche, J. Nikkinen, S.-M. Huttula, H. Aksela, M. Huttula, and S. Aksela, Phys. Rev. A **75**, 012501 (2007).
[33] A. F. Starace, in *Handbuch der Physik*, edited by W. Mehlhorn (Springer, Berlin, 1982), Vol. 31, p. 1.
[34] J. Cooper and R. N. Zare, J. Chem. Phys. **48**, 942 (1968).
[35] D. A. Varshalovich, A. N. Moskalev, and V. K. Khersonskii, *Quantum Theory of Angular Momentum* (World Scientific, Singapore, 1988).
[36] V. V. Balashov, A. N. Grum-Grzhimailo, and N. M. Kabachnik, *Polarization and Correlation Phenomena in Atomic Collisions* (Kluwer Academic/Plenum Publishers, New York, 2000).
[37] A. Verweyen, A. N. Grum-Grzhimailo, and N. M. Kabachnik, Phys. Rev. A **60**, 2076 (1999).
[38] A. N. Grum-Grzhimailo and M. Meyer, Eur. Phys. J. Spec. Top. **169**, 43 (2009).
[39] A. Dorn, J. Nienhaus, M. Wetzstein, C. Winnewisser, W. Mehlhorn, V. V. Balashov, A. N. Grum-Grzhimailo, N. M. Kabachnik, and O. I. Zatsarinny, J. Phys. B **27**, L529 (1994).
[40] Ph. Wernet, J. Schulz, B. Sonntag, K. Godehusen, P. Zimmermann, A. N. Grum-Grzhimailo, N. M. Kabachnik, and M. Martins, Phys. Rev. A **64**, 042707 (2001).
[41] C. Froese Fischer, T. Brage, and P. Jönsson, *Computational Atomic Structure: An MCHF Approach* (IOP Publishing, Bristol, 1997).
[42] The sum $I(\varphi_a)+I(\varphi_a+90)$ is also independent of the angle φ_a, as follows from Eq. (12).